FULL PAPER

Magnetic Resonance in Medicine 000:000–000 (2012)

Contrast Enhanced Lung MRI in Mice Using Ultra-Short Echo Time Radial Imaging and Intratracheally Administrated Gd-DOTA-Based Nanoparticles

Andrea Bianchi,[1] François Lux,[2] Olivier Tillement,[2] and Yannick Crémillieux[1]*

Purpose: To investigate the in vivo T_1-enhancement of the lung parenchyma in free-breathing healthy mice following intratracheal administration of Gd-DOTA-based nanoparticles, to assess the enhancement kinetics of the instilled contrast medium and to identify its elimination pathways.

Methods: Ultrashort Echo Time (276 μs) proton MRI of the lung was performed (N = 14) at 4.7 T after the intratracheal instillation of 50 μL of seven different concentrations of contrast agent solution (from 2 to 100 mM of Gd^{3+}). The signal enhancement (SE) in lungs, blood, liver, kidneys, and bladder was assessed (N = 3) for a 50 mM concentration solution at different time points.

Results: The largest SE in lungs (266 ± 14%) was observed for a 50 mM solution of Gd^{3+}. In lungs, the SE was observed to decay exponentially with a time constant of 149 ± 51 min. The passage of the nanoparticles from lung tissue to blood and kidneys, and ultimately to the bladder, was observed. No significant hepatic enhancement was measured.

Conclusion: This study demonstrates the feasibility of large SEs of lung tissue using intratracheally administrated solutions of Gd-based contrast agents. In future applications, the SE in lungs could be used to image the biodistribution of coadministrated drug aerosols or to selectively enhance lung diseased tissues. **Magn Reson Med 000:000-000, 2012. © 2012 Wiley Periodicals, Inc.**

Key words: lung proton MRI; UTE; gadolinium; contrast agent; nanoparticles

INTRODUCTION

In a pioneering work, two decades ago, Berthezène et al. (1,2) demonstrated the possibility of increasing the signal to noise ratio (SNR) in rat lungs following aerosolization of Gd-DTPA and investigated the elimination pathways and biodistribution kinetics of the Gd-DTPA aerosol. However, due to the limitations in lung MR imaging at that time, these studies had few subsequent development and applications (3–6).

With the advent of Ultra-short Echo Time (UTE) sequences, the interest for lung proton MRI has recently increased since the first pioneering studies using radial acquisitions in lungs (7,8). Indeed, in small animals radial UTE sequences can efficiently limit the negative impact on image quality of low proton density, multiple air/tissue interfaces, and respiratory and cardiac motion artifacts that characterize the lungs. As a result, radial UTE acquisitions can provide lung images in small animals at submillimetric resolution with significant SNR (9–11).

At the same time in the last two decades, the design of new contrast agents has been actively pursued towards multimodality (12–15), multivalency (16), combined therapeutic and imaging properties (17), or active targeting with the use of ligand peptides (18).

Among the different possible approaches for contrast agent delivery to the lung, the intratracheal instillation appears as a promising route of administration in animal experimentation. Several advantages of this technique have been extensively described in literature (19–21); between them, the possibility of delivering a well known dose directly to the lungs, of determining the approximate dose range that may be appropriate for later studies and of obtaining highly localized exposures to specific lobes of the lungs (leaving the other lobes as controls) are of particular interest.

In the light of these considerations, an UTE MRI investigation of the T_1-enhancement of the lung parenchyma in free-breathing mice following intratracheal administration of a Gd-DOTA-based contrast agent is reported in this article. The temporal evolution of the signal enhancement (SE), related to the biodistribution of the contrast agent in different organs, is also described to assess the enhancement kinetics and to identify the elimination pathways.

METHODS

Contrast agents

The contrast agents used in this study are referred as ultra-small rigid platforms (USRPs). They are obtained after a slow dissolution of a gadolinium oxide core, encapsulated in a hollow sphere of polysiloxane, in presence of chelating species like DOTA. The resulting molecules are composed of a polysiloxane backbone with, on average, about 10 Gd-DOTA species grafted via amide

[1]Centre de Recherche Cardio-Thoracique de Bordeaux, U1045, Université Bordeaux Segalen, Bordeaux, France.

[2]Laboratoire de Physico-Chimie des Matériaux Luminescents, Université de Lyon 1, Lyon, France.

Grant sponsors: European Network PINET and Agence Nationale de la Recherche; Grant number: FP7-PEOPLE-2010-ITN-264864 and ANR-12-P2N-0009.

*Correspondence to: Yannick Crémillieux, Ph.D., Université Bordeaux Segalen, U1045, Bât TP, 146, rue Léo-Saignat, 33076 Bordeaux Cedex, France. E-mail: yannick.cremillieux@u-bordeaux2.fr

Received 23 April 2012; revised 8 October 2012; accepted 11 November 2012.

DOI 10.1002/mrm.24580
Published online in Wiley Online Library (wileyonlinelibrary.com).

functions. The distribution of the USRPs hydrodynamic diameters is entirely below 5.5 nm, with an average size of 3.0 ± 0.1 nm. Due to the smaller rotation rate, the longitudinal relaxivity per gadolinium atom, r_1 = 11.4 mM^{-1} s^{-1} at 1.4 T, is about three times higher compared with standard Gd-DOTA and Gd-DTPA molecules. The relaxivity per USRP particle is equal to 114 mM^{-1} s^{-1} at 1.4 T. The half-life of the particles in blood is equal to 9 min. The hepatic uptake, following intravenous injection, was measured below 0.15% of the injected dose through SPECT imaging. More details about the synthesis and the properties of these USRPs can be found in Ref. 13.

Animals

Female Balb/c mice (N = 24), 6 week-old weighting 20–22 g were purchased from Elevage Janvier (Le Genest, Saint Isle, France). Before the experiment, the animals were acclimatized in a temperature-controlled environment for 1 week. Experiments were carried out following the INSERM (Institut National de la Santé et de la Recherche Médicale) guidelines regarding the fair treatment of animals.

Protocol

Enhancement-Concentration Study

Mice were anesthetized using an intraperitoneal injection of 50 μg g^{-1} ketamine (Panpharma, Fougères, France) and 5 μg g^{-1} xylazine (Sigma-Aldrich, Saint-Quentin-Fallavier, France). After the acquisition of MR baseline images, an orotracheal intubation was performed on the mice with a 22-Gauge Teflon intravenous catheter. The bilateral instillation was performed passing the catheter through the vowel cords into the beginning of the trachea, before the carina. A volume of 50 μL solution of Gd-DOTA-based contrast agent was obtained dissolving the nanoparticles in saline solution (0.9% NaCl) to reach the desired concentrations and was introduced in the lungs through the tracheal catheter, allowing diffusion in both the primary bronchi and consequently in both the lungs. Seven different concentrations (expressed in Gd^{3+}) were investigated (2, 5, 10, 20, 33, 50, and 100 mM). Each animal (N = 14 in total and N = 2 for each concentration) received only one dose of contrast agent while saline solution was administrated to two control mice (N = 2). After the extubation, MR images of the mice lungs were acquired at different times, from 5 min up to a few hours.

Follow-Up Study

The concentration was fixed to 50 mM and the administration procedure was repeated on the rest of the animals (N = 3). For these mice, MR images of the lungs, liver, kidneys, and bladder were acquired at different times, from 5 min up to 2 days after the contrast agent administration.

MRI

The images were acquired with a 4.7 T Biospec 47/50 spectrometer (Bruker, Ettlingen, Germany), using a transmitter/receiver quadrature coil of 25 mm inner diameter (Bruker, Ettlingen, Germany). Mice were placed prone in a custom-built plastic holder (optimized for allowing an accurate positioning of the mice inside the scanner) and kept anesthetized with 2% isoflurane in a mixture of N_2/O_2 (80:20) via facial mask. The body temperature was kept constant using warm circulating water and the respiratory cycle was monitored constantly.

During the investigation, images of the mice were acquired at different times with long intervals in-between (especially in the case of the follow-up study). In the intervals between the acquisitions, animals were extracted from the spectrometer and left in a temperature-controlled environment where they were allowed to recover. Before the acquisition of the succeeding images, mice were anesthetized with isoflurane at 2% and repositioned in the scanner. A fast FLASH sequence (axial, sagittal, and coronal planes) was acquired to control the correct positioning of the animals, checking the main anatomical landmarks available (heart, spinal cord, and lungs); a correction of the position inside the spectrometer was applied when needed.

The whole procedure allowed acquiring images over a long period without altering the vital functions of the animals.

Optimization Study

An optimization study was performed in a separate set of mice (N = 4) to determine the repetition time (TR) and the flip angle (FA) to be used during the enhancement-concentration and the follow-up studies. TRs of 14, 50, 84, and 200 ms were investigated before and after the administration of a 50 mM contrast agent solution in N = 2 mice, keeping the FA constant (60°). The same procedure was repeated on other N = 2 mice, exploring FAs of 30°, 60°, and 80° and keeping the TR constant (84 ms). The other sequence parameters and the imaging protocol were identical to those used for the enhancement-concentration and follow-up studies, as detailed below. After this study, the optimized TR and FA were kept constant during the present investigation.

Enhancement-Concentration Study

For each animal, 6 axial slices of 1 mm thickness were acquired (with an inter-slice distance of 2 mm). The acquisition was performed in free-breathing animals, using a 2D multislice UTE sequence (804 directions/128 points, 4 averages) with a TE of 276 μs, bandwidth of 50 kHz and field of view (FOV) of 3 × 3 cm^2. Free induction decay acquisition was started during read gradient ramping, immediately after the Gaussian-shaped RF slice excitation (duration 0.3 ms) and the slice refocusing gradient. The total acquisition time was of about 4 min.

Follow-Up Study

For each animal, 6 axial slices of 1 mm thickness were acquired (with an inter-slice distance of 2 mm) to image the lungs and the liver. The acquisition was performed in free-breathing animals, using a 2D multislice UTE sequence (804 directions/128 points, 1 average) with a TE of 276 μs, bandwidth of 50 kHz, FOV of 3 × 3 cm^2,

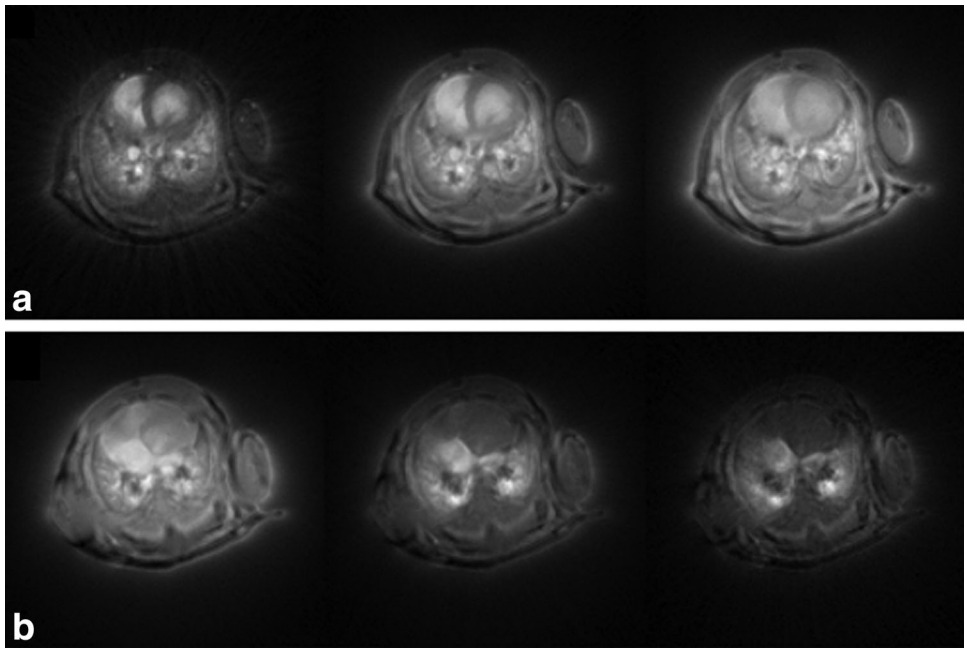

FIG. 1. Exemplary axial slices of the mouse lungs 25 min after the administration of the contrast agent for different (a) TRs (from left, respectively, 14, 50, and 84 ms) and (b) FAs (from left, respectively, 30°, 60°, and 80°).

TR of 84 ms for a total acquisition time of about 1 min; the FA was fixed at 60°.

Similarly, for each animal, 10 coronal slices of 1 mm thickness were acquired to image the kidneys and the bladder, using a 2D multislice FLASH sequence (matrix size 256 × 256, 1 average) with TE of 2.3 ms, bandwidth of 100 kHz, FA of 60°, FOV of 3 × 6 cm^2 and TR of 100.5 ms for a total acquisition time of about 25 s.

High Resolution Acquisition

One additional mouse ($N = 1$) received a selective instillation of 50 μL of contrast agent solution (50 mM concentration) in the left lung. The unilateral instillation procedure is the same as the bilateral one but the catheter is pushed further into the trachea to reach the beginning of the left primary bronchus. Fourteen axial slices of 0.5 mm thickness were acquired (with an interslice distance of 0.7 mm) to image the lungs with high-resolution. The acquisition was performed in free-breathing condition, using a 2D multislice UTE sequence (804 directions/128 points, 4 average) with a TE of 276 μs, bandwidth of 50 kHz, FA of 60°, FOV of 2.5 × 2.5 cm^2 and TR of 200 ms, for a total acquisition time of about 10 min.

Image Reconstruction and Analysis

The images acquired with the UTE sequence were reconstructed and analyzed with an in-house software implemented in IDL (RSI, Boulder, CO). Following the application of a regridding algorithm and a weighting function (22), the images were interpolated to a 256 × 256 image matrix. The images acquired with the FLASH sequence were reconstructed and analyzed with the Bruker ParaVision 5.1 software.

For each image, the organs of interest were manually segmented to measure the total average signal. The noise of the images was quantified as the standard deviation of the mean signal of a region of interest (ROI) selected in the image background and the SNR was computed. The SE in each image was computed as the difference between the SNR in the lungs after the contrast agent administration and before (baseline images), normalized to the SNR of the baseline images (23). All the regions of interest in the lungs were drawn avoiding the main visible vessels.

Optimization Study

For each TR, the SNR of the lung parenchyma was evaluated on three axial slices (apex, central, and basal regions of the lungs) before the administration of the contrast agent and averaged over the two lungs and the two mice. For each FA, the SNR of the lung parenchyma was evaluated as described for the TR optimization while the SE was evaluated on the same three axial slices after the administration of the contrast agent and averaged over the two lungs and the two mice.

Enhancement-Concentration Study

For each concentration, the SE of the lungs was evaluated on three axial slices (apex, central, and basal

Table 1
Numeric Values (Mean ± S.E.M.) for the Optimization Study

TR optimization			FA optimization		
TR (ms)	Acquisition time (s)	SNR	FA (°)	SNR	SE (%)
14	45	18 ± 3	30	37 ± 3	64 ± 5
50	160	31 ± 4	60	31 ± 3	200 ± 15
84	270	36 ± 4	80	24 ± 3	273 ± 28
200	643	40 ± 5			

Among the TRs explored, 84 ms was chosen as the best compromise between the SNR before the administration of the contrast agent and the total acquisition time. Among the FAs explored, 60° was chosen as the best compromise between the SNR and the contrast before the administration of the USRPs and the SE achievable after the instillation of the nanoparticles.

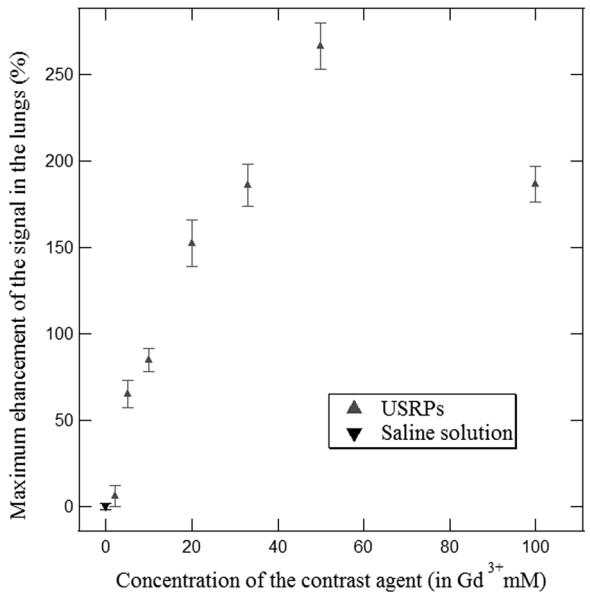

FIG. 2. Maximum SE obtained for different concentrations of contrast agent and saline solution. The values are averaged over the three slices analyzed and the two lungs (mean ± S.E.M). The increase in the SE reaches its maximum for a 50 mM contrast agent solution; a further increase in the concentration causes a decrease in the SE.

regions of the lungs) and averaged over the two organs and the two mice.

Follow-Up Study

For each image, the lungs (left and right), kidneys (left and right), liver, vena cava, bladder, and left ventricle were manually segmented. For each mouse, the SE was evaluated on three axial slices (center and bottom of the lungs and liver) and four coronal slices (two for the kidneys and two for the bladder). For each animal, the SE was averaged over the different measured slices.

RESULTS

The optimization study on TRs and FAs was conducted to find the best parameters to be used during the enhancement and follow-up investigations. In Figure 1, exemplary axial slices acquired with the UTE sequence 25 min after the administration of a 50 mM contrast agent solution are shown for different TRs (Fig. 1a) and FAs (Fig. 1b). Among the TRs explored (14, 50, 84, and 200 ms) a TR of 84 ms was chosen for the present investigation as the best compromise between the SNR (>35 in the lungs before contrast agent instillation) and the total acquisition time (about 4 min); among the FAs studied (30°, 60°, and 80°) a FA of 60° was chosen since it provided good SNR and contrast before the administration of the contrast agent and high SE after the instillation (see Table 1 for the numeric data).

After having found the optimal parameters, the enhancement-concentration relationship was investigated. The SE measured at different times in the control mice always kept close to zero (0.2 ± 2.1%) as for the one measured in the mice which received a 2 mM Gd-DOTA-based contrast agent solution (6.5 ± 5.9%). On the contrary, for instilled contrast agent solutions with a concentration equal or higher than 5 mM, already a few minutes after the administration (from 5 to 25 min) mice presented a significant SE (ranging from 65 ± 8% for the 5 mM solution to 266 ± 14% for the 50 mM one).

The plot of Figure 2 shows the maximum SE measured for each contrast agent concentration. The SE due to the Gd T_1-shortening effect is increasing with the concentration of the contrast agent administrated to the mice up to 50 mM. A maximum SE of 266 ± 14% was reached with 50 μL of a 50 mM solution (Fig. 3), while an inferior enhancement (186 ± 10%) is reached with the 100 mM solution.

In Figure 4, the temporal evolution of the maximum SEs in the lungs for a 50 mM solution is shown. A mono-exponential fit provides an estimate of the time required to reduce to 63% of the signal intensity of the MR SE due the contrast agent administrated intratracheally to the mice ($\tau = 149 \pm 51$ min).

The passage of the nanoparticles from the lungs to the vascular system and to the kidneys is illustrated in Figures 5 and 6. A significant SE (>80%) is already visible 10–15 min after the administration of the contrast agent. The enhancement keeps roughly constant for about 2 h and starts to decrease slowly after. The contrast agent

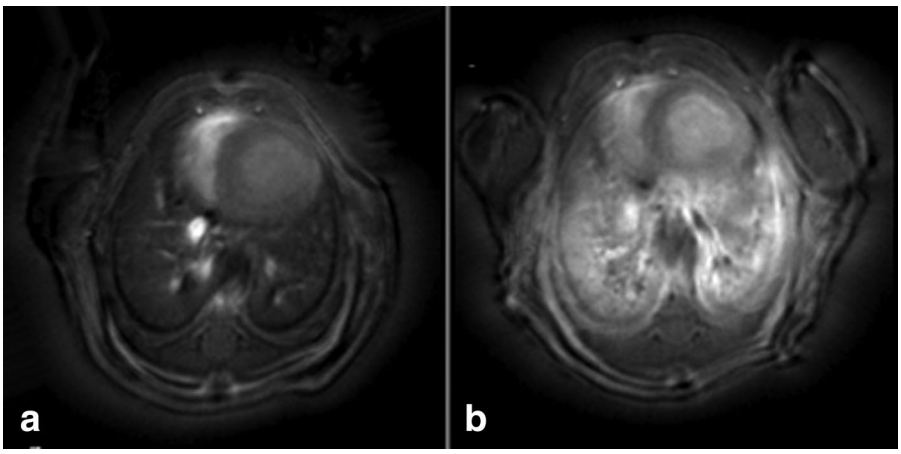

FIG. 3. One of the six axial slices of the mouse lungs before (a) and after (b) the intratracheal administration of 50 mM Gd contrast agent. The images, acquired with a UTE sequence (FA of 60°, FOV of 3 cm), show an enhancement superior to 266% in the lung parenchyma.

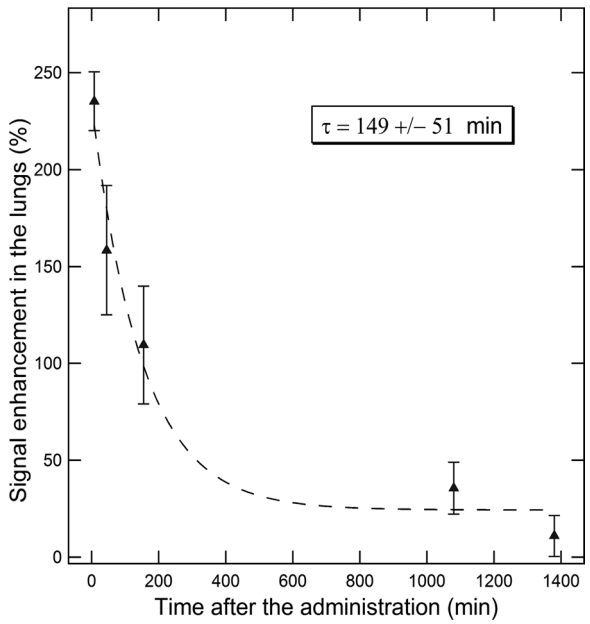

FIG. 4. SE temporal evolution obtained in the lungs with the 50 mM solution (mean ± S.E.M.). The exponential fit provides an estimate of the time required to reduce the MR contrast agent SE of 63% of its initial value.

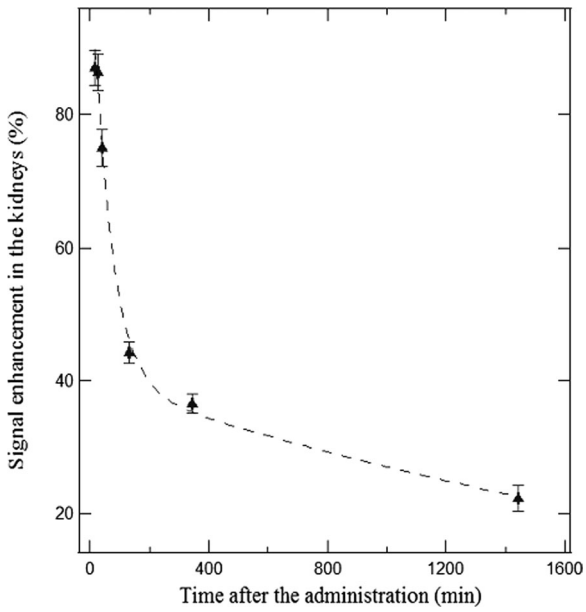

FIG. 6. SE temporal evolution obtained in the kidneys with the 50 mM solution. The values are averaged over the two slices analyzed and the two kidneys (mean ± S.E.M.). The presence of the nanoparticles in the kidneys can be detected 24 h after the intratracheal administration.

can still be detected in the kidneys 24 h after the instillation.

The elimination path of the contrast agent ends up when the nanoparticles pass from the kidneys to the bladder and are removed through urine (Fig. 7). A bigger variability than for the lungs and the kidneys was observed in the SE of the bladder due to the variable amount of urine. SEs bigger than 130% can be seen already 10–15 min after the initial administration while enhancements of more than 700% are reached after about 2 h, as shown in Figure 8. A significant SE (>80%) can still be seen 24 h after the instillation.

No significant hepatic enhancement was observed: the SE in the liver kept always lower than 15%. While the SEs measured in the vena cava are negligible (<15%), enhancements up to 65% were measured in the heart (left ventricle).

DISCUSSION

As previously demonstrated, radial MR sequences are less sensitive to cardiac and respiratory motion (24) than Cartesian MR acquisitions. Despite the absence of cardiorespiratory gating, a good spatial resolution was reached as can be seen from Figure 9, where bronchi with diameter of a few hundreds of microns can be visualized. This result is in agreement with published works on UTE sequences properties. For example, Zurek et al. (11) showed that, with radial acquisitions, equivalent spatial resolutions in mice could be obtained using cardiorespiratory gating acquisitions or averaging approaches.

Consequently, the free-breathing acquisition in mice can be used, with limited impact on image quality and spatial resolution, to maintain a constant TR and a steady-state regime and to keep the total acquisition time

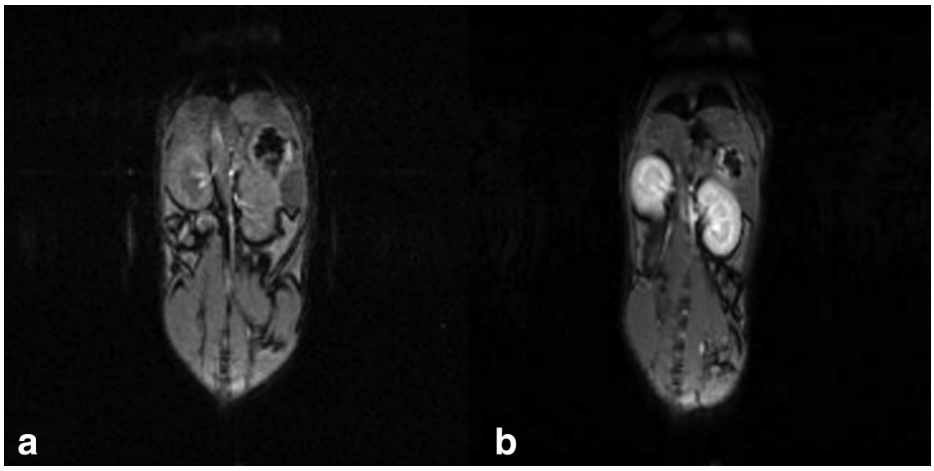

FIG. 5. Coronal images of the kidneys before (a) and 290 min after (b) the intratracheal administration of 50 mM Gd contrast agent. The images are acquired with a FLASH sequence (FA of 60°, FOV of 3 × 6 cm^2). An enhancement superior to 80% can be measured.

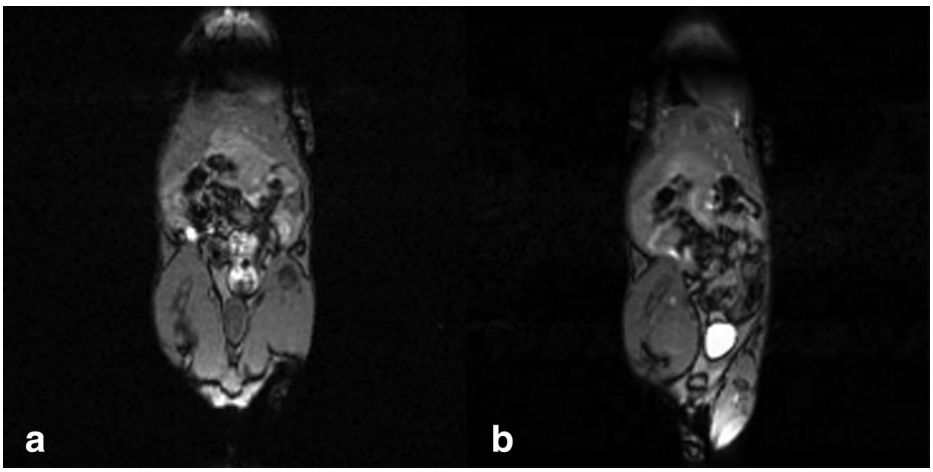

FIG. 7. Coronal images of the bladder before (a) and 290 min after (b) the intratracheal administration of 50 mM Gd contrast agent. The images are acquired with a FLASH sequence (FA of 60°, FOV of 3 × 6 cm^2). An enhancement superior to 700% can be measured due to the high concentration of the nanoparticles in the small bladder.

compatible with small animal scanning. This constant TR is mandatory for an accurate measurement of the change in signal intensity due to the presence of the contrast agent while the short acquisition times are needed in order to be compatible with biodistribution imaging of the contrast agent in small animals.

Two main applications of combined UTE sequences and intratracheally administered positive contrast agent can be envisioned for enhanced lung proton MRI. The first one is related to the increase of SNR in lungs that can be obtained with a T_1-weighted in vivo UTE MR sequence, as used in the present investigation. Considering the low proton spin density in lungs, averaging in lung MRI is necessary and short TRs are required to reduce the total acquisition time. The shortening of T_1 relaxation times is thus an efficient way to improve the image SNR per unit time. Following instillation of 50 mM solution of USRPs contrast agent, the mean SNR in lungs increased from 35 to 128. A peculiar situation was observed with the administration of highly concentrated solutions (100 mM). In this case, the time required to reach the maximum SE is significantly superior (3–4 times more) compared with lower concentrations. It is hypothesized that for high concentration of USRPs, the signal decay due to shortened T_2^* cannot be neglected anymore until a lower concentration of the contrast agent in the lung is reached following gradual elimination of the nanoparticles via the kidneys.

The second application, certainly of greater interest, concerns the possibility of generating specific contrast mechanisms in lungs. For instance, as proposed and demonstrated previously with gadolinium aerosols, the changes in signal intensity can be related to the lung ventilation (1,3). Alternatively, coadministration of aerosolized drugs and contrast agents could be used to quantify, localize, and monitor the distribution of inhaled biopharmaceuticals in lungs (21).

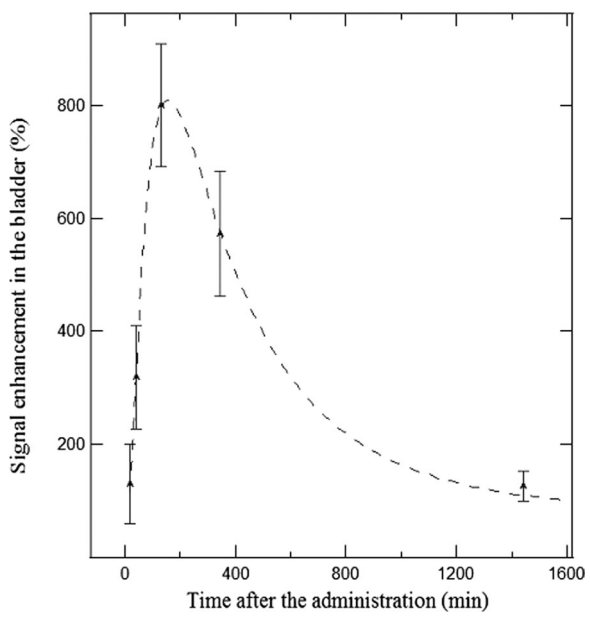

FIG. 8. SE temporal evolution obtained in the bladder with the 50 mM solution (mean ± S.E.M.). The nanoparticles are still present in the bladder 24 h after the intratracheal administration.

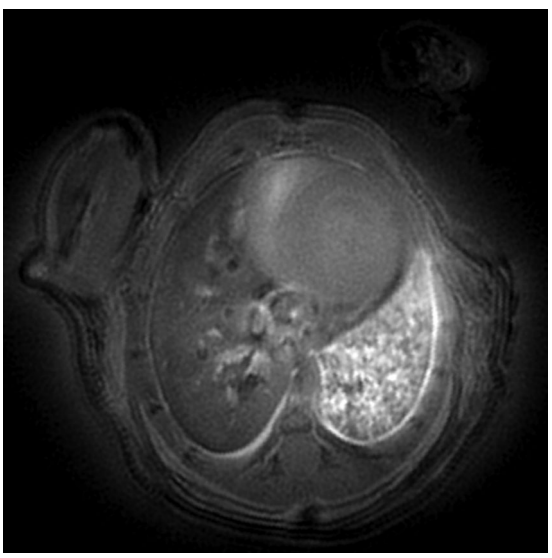

FIG. 9. One of the 14 high resolution axial slices of the mouse lungs after the intratracheal administration of 50 mM Gd contrast agent in the left lung. The image, acquired with a UTE sequence (slice thickness of 0.5 mm, FOV of 2.5 × 2.5 cm^2), show the typical resolution reachable. The main bronchi and the peribronchial wall can be identified in the image.

In this study, we chose more specifically to investigate the relaxation properties and the biodistribution following administration in lungs of ultra-small particles designed for diagnostic multimodal imaging and for therapeutic applications (13).

Some of the prerequisites for successful applications of intratracheal contrast agent for lung MR imaging are an appropriate biodistribution and clearance of the nanoparticles and a good detection sensitivity of the contrast medium.

From the MRI images and the SE curves, a fast passage of the contrast agent solution from the airways to the lung tissue then to the kidneys and eventually to the bladder for urine elimination was observed. However, no significant change in signal intensity was noticed in the liver. These observations are coherent with the previously reported ability of the USPRs to escape phagocytosis by macrophages and monocytes (13). Lux et al., in fact, showed that identical USPRs follow the renal clearance route also in case of intravenous injection, escaping the mononuclear phagocytic system. All these findings can be explained at the light of the ultrasmall hydrodynamic diameters of the nanoparticles. As Choi et al. have recently demonstrated using near-infrared florescence imaging (25), between the physicochemical properties (shape, size, chemical composition, and surface charge), the hydrodynamic diameters of the nanoparticles is the fundamental factor which affects trafficking across the alveolar surface barrier into tissue and once there, their biodistribution and clearance; particles with hydrodynamic diameters inferior to 6 nm showed the capability to quickly enter the bloodstream from the alveolar airspaces and were cleared from the body by means of renal filtration. Similar conclusions were found in the case of intravenous administration (26).

The presence of contrast agent was detectable in arterial blood (left ventricle) but not in venous blood. The nanoparticles pass from the alveolar space into the lung tissue and in the arterial bloodstream, arriving in very short times in the left heart through the pulmonary vein and generating a visible SE. Once there, the nanoparticles enter the systemic circulation, diffusing in the rest of the blood. In this phase, the USRPs are diluted in the whole mouse blood volume ($\approx$1.2–1.6 mL) and undergo a systematic renal clearance. These two concurrent phenomena may explain why no SE is measured in the venous blood. Furthermore, considering that at 4.7 T the average T_1 for the venous blood is 1.37 s while for the arterial blood is 1.7 s (27), it is clear that the percentage change in the venous blood signal would be lower than for the arterial one.

The relatively long residence time ($>$2 h) of the contrast agent in the lungs, the homogeneous distribution of the nanoparticles in the parenchyma and their ability of escaping alveolar macrophages phagocytosis can be considered as good premises for a substantial accumulation of the nanoparticles in diseased lung tissues. As Roa et al. (28) have shown, in fact, the administration route of the nanoparticles strongly influence the effectiveness of the contrast agent and the macrophage uptake is one of the main limiting factors in the theranostic potential of a given nanocarrier. Furthermore, the favorable pharmacokinetics of the USRPs, eliminated through renal clearance, which follow predictable rules and is quite fast (26,29), ensure negligible retention in the reticuloendothelial system and hence the substantial nontoxicity of the contrast agent (26,28,29).

The instillation administration modality used in this study has the main advantage, compared with the nebulization administrations, of delivering to the lungs in a short time an amount of solution known with good precision (19–21). As a consequence, an accurate measurement of the relationship enhancement-concentration was carried out. A feasibility study (data not presented here) has shown that the instilled volume of contrast agent solution can be reduced up to 30 μL without any substantial change in the results described in the present investigation. A further decrease in the administrated volume, however, seems to lead to inhomogeneities in the nanoparticle distribution in the lungs. For these reasons, in the future, intratracheal nebulization and aerosol will be investigated as potential improvements of contrast agent biodistribution in the lungs with lower volumes.

CONCLUSION

The radial UTE technique was successfully applied to detect large (about four-fold increase in SNR) and lasting ($>$2 h) changes in the MRI signal coming from the lungs of free-breathing healthy mice, before and after the intratracheal administration of a Gd-DOTA-based contrast agent. The study of the SEs evolution in time after the administration of the contrast agent has allowed detecting the elimination pathway of the administrated nanoparticles.

The MRI measurements have confirmed that the size of the nanoparticles is small enough to ensure a renal elimination and a negligible hepatic uptake, making the contrast agent and the instillation protocol good candidates for future application in diagnostic imaging and investigation of diseased lungs.

ACKNOWLEDGMENTS

The authors are grateful to Gérard Raffard and Dr. Bassem Hiba for advices and help in use of the MR scanner. They thank Dr. Sylvain Miraux for providing the mouse RF coil.

REFERENCES

1. Berthezène Y, Vexler V, Clément O, Mühler A, Moseley ME, Brasch RC. Contrast-enhanced MR imaging of the lung: assessments of ventilation and perfusion. Radiology 1992;183:667–672.
2. Berthezène Y, Mulher A, Lang P, Shames D, Clement O, Rosenay W, Kuwatsuru R, Brasch R. Safety aspects and pharmacokinetics of inhaled aerosolized Gadolinium. J Magn Reson Imaging 1993;3: 125–130.
3. Haage P, Karaagac S, Adam G, Glowinski A, Günther RW. Comparison of aerosolized gadoteridol and gadopentetate dimeglumine for magnetic resonance ventilation imaging of the lung. Magn Reson Med 2001;46:803–806.
4. Suga K, Yuan Y, Nobuhiko O, Okada M, Kawakami Y, Matsunaga N. Potential of magnetic resonance lymphography with intrapulmonary

injection of gadopentetate dimeglumine for visualization of the pulmonary lymphatic basin in dogs: preliminary results. Invest Radiol 2003;38:679–689.
5. Sood BG, Shen Y, Latif Z, Chen X, Sharp J, Neelavalli J, Joshi A, Slovis TL, Haacke EM. Aerosol delivery in ventilated newborn pigs: an MRI evaluation. Pediatr Res 2008;64:159–164.
6. Mosbah K, Ruiz-Cabello J, Berthezène Y, Crémillieux Y. Aerosols and gaseous contrast agents for magnetic resonance imaging of the lung. Contrast Media Mol Imaging 2008;3:173–190.
7. Bergin CJ, Pauly JM, Macovski A. Lung parenchyma: projection reconstruction MR imaging. Radiology 1991;179:777–781.
8. Bergin CJ, Noll DC, Pauly JM, Glover GH, Macovski A. MRI imaging of lung parenchyma: a solution to susceptibility. Radiology 1992;183: 673–676.
9. Gewalt SL, Glover GH, Hedlund LW, Cofer GP, MacFall JR, Johnson GA. MR microscopy of the rat lung using projection recostruction. Magn Reson Med 1993;29:99–106.
10. Johnson GA, Cofer GP, Hedlund LW, Maronpot RR, Suddarth SA. Registered 1H and 3He magnetic resonance microscopy of the lung. Magn Reson Med 2001;45:365–370.
11. Zurek M, Bessaad A, Cieslar K, Crémillieux Y. Validation of simple and robust protocols for high-resolution lung proton MRI in mice. Magn Reson Med 2010;64:401–407.
12. Lewin M, Carlesso N, Tung CH, Tang XW, Cory D, Scadden DT, Weissleder R. Tat peptide-derivatized magnetic nanoparticles allow in vivo tracking and recovery of progenitor cells. Nat Biotechnol 2000;18:410–414.
13. Lux F, Mignot A, Mowat P, et al. Ultrasmall rigid particles as multimodal probes for medical applications. Angew Chem 2011;123: 12507–12511.
14. Kim JS, Kim YH, Kim JH, et al. Development and in vivo imaging of a PET/MRI nanoprobe with enhanced NIR fluorescence by dye encapsulation. Nanomedicine 2012;7:219–229.
15. Alric C, Taleb J, Le Duc G, et al. Gadolinium chelate coated gold nanoparticles as contrast agents for both X-ray computed tomography and magnetic resonance imaging. J Am Chem Soc 2008;130: 5908–5915.
16. Jin ZH, Josserand V, Foillard S, Boturyn D, Dumy P, Favrot MC, Coll JL. In vivo optical imaging of integrin α_V-β_3 in mice using multivalent or monovalent cRGD targeting vectors. Mol Cancer 2007; 6:41.
17. Le Duc G, Miladi I, Alric C, et al. Toward an image-guided microbeam radiation therapy using gadolinium-based nanoparticles. ACS Nano 2011;5:9566–9574.
18. Benezra M, Penate-Medina O, Zanzonico PB, et al. Multimodal silica nanoparticles are effective cancer-targeted probes in a model of human melanoma. J Clin Invest 2011;121:2768–2780.
19. Driscoll KE, Costa DL, Hatch G, Henderson R, Oberdorster G, Salem H, Schlesinger RB. Intratracheal instillation as an exposure technique for the evaluation of respiratory tract toxicity: uses and limitations. Toxicol Sci 2000;55:24–35.
20. Costa DL, Lehmann JR, Winsett D, Richards J, Ledbetter AD, Dreher KL. Comparative pulmonary toxicological assessment of oil combustion particles following inhalation or instillation exposure. Toxicol Sci 2006;91:237–246.
21. Shoyele SA, Cawthome S. Particle engineering techniques for inhaled biopharmaceuticals. Adv Drug Deliv Rev 2006;58:1009–1029.
22. Jackson JI, Meyer CH, Nishimura DG, Macovski A. Selection of a convolution function for Fourier inversion using gridding. IEEE Trans Med Imaging 1991;10:473–478.
23. Armitage P, Behrenbruch C, Brady M, Moore N. Extracting and visualizing physiological parameters using dynamic contrast-enhanced magnetic resonance imaging of the breast. Med Image Anal 2005;9: 315–329.
24. Glover GH, Pauly JM. Projection reconstruction techniques for reduction of motion effects in MRI. Magn Reson Med 1992;28:275–289.
25. Choi HS, Ashitate Y, Lee JH, et al. Rapid translocation of nanoparticles from the lung airspaces to the body. Nat Biotech 2010;28: 1300–1303.
26. Choi HS, Liu W, Liu F, Nasr K, Misra P, Bawendi MG, Frangioni JV. Design considerations for tumour-targeted nanoparticles. Nat Nano 2010;5:42–47.
27. Silvennoinen MJ, Kettunen MI, Kauppinen RA. Effects of hematocrit and oxygen saturation level on blood spin-lattice relaxation. Magn Reson Med 2003;49:568–571.
28. Roa WH, Azarmi S, Al-Hallak MK, Finlay WH, Magliocco AM, Löbenberg R. Inhalable nanoparticles, a non-invasive approach to treat lung cancer in a mouse model. J Control Release 2011;150:49–55.
29. Choi HS, Liu W, Misra P, Tanaka E, Zimmer JP, Itty Ipe B, Bawendi MG, Frangioni JV. Renal clearance of nanoparticles. Nat Biotech 2007;25:1165–1170.